Bipolar Resistance Switching in Pt/CuO_x/Pt via Local Electrochemical Reduction

Kenneth D'Aquila,[1,2] Charudatta Phatak,[1] Martin V. Holt,[3] Benjamin D. Stripe,[3] Sheng Tong,[3] Woon Ik Park,[1] Seungbum Hong[1*] and Amanda K. Petford-Long[1,2]

[1]*Materials Science Division, Argonne National Laboratory, Lemont, IL 60439, USA*
[2]*Department of Materials Science and Engineering, Northwestern University, Evanston, IL, 60208, USA*
[3]*Nanoscience and Technology Division, Argonne National Laboratory, Lemont, IL 60439, USA*

Abstract

The local changes in copper oxidation state and the corresponding resistance changes in Pt/CuO_x/Pt nanoscale heterostructures have been investigated using x-ray nanoprobe spectro-microscopy and current-voltage characterization. After gentle electroforming, during which the current-voltage behavior remains non-linear, the low resistance state was reached and we observed regions of 160 nm width that show an increase in Cu K-alpha fluorescence intensity, indicative of partial reduction of the CuO_x. Analysis of the current voltage curves showed that the dominant conduction mechanism is Schottky emission and that the resistance state is correlated with the Schottky barrier height. We propose that the reversible resistivity change in these Pt/CuO_x/Pt heterostructures occurs through local electrochemical reduction leading to change of the Schottky barrier height at the interface between Pt and the reduced CuO_x layers and to change of the CuO_x resistivity within laterally confined portions of the CuO_x layer. These experiments reveal important insights into the mechanism of resistance switching of Pt/CuO_x/Pt performed in a current and voltage regime that does not create a metallic conduction path.

[*]Author to whom correspondence should be addressed. Electronic mail: hong@anl.gov

Resistance switching in metal/insulator/metal heterostructures is a process by which an applied electric field reversibly changes the electrical resistance across the oxide between two or more states.[1–4] Many research groups have explored the physical origins of this phenomenon and have constructed resistance change based memory devices or bio-inspired artificial neuron devices.[5,6] There has also been a wide range of proposed mechanisms. These can be classified as being primarily electronic, ionic, or thermal in origin.[7] These mechanisms can result in the formation of a conducting bridge phase, a change in the energy barrier at the metal/insulator interface, or both.[6]

Heterostructures containing copper oxide have shown repeatable resistance switching and typically involve a high resistance state (HRS) that is two or three orders of magnitude larger than the low resistance state (LRS).[8] Additionally, the LRS typically displays Ohmic conduction while a variety of leakage current mechanisms have been proposed for the high resistance state (HRS).[9] Considerable progress has been made in identifying the chemical changes that result from the resistance switching process within Pt/CuO_x/Pt heterostructures. Drift of oxygen vacancies through the CuO_x layer plays an important role and the contribution of oxygen vacancies have been explored using *in-situ* transmission electron microscopy (TEM) analysis and photoemission electron microscopy (PEEM).[10,11] These studies proposed that the LRS results from the formation of conductive copper-rich CuO_x (a mixture of Cu and Cu_2O) bridge regions.[10,11] After switching back to the HRS, re-oxidized CuO_x regions were found near the metal electrode.[15]

The goal of our study is to explore the mechanisms by which resistance switching occurs in a current regime before metallic conduction paths are fully formed. We have explored this question by studying the resistance switching mechanisms of Pt/CuO_x/Pt heterostructures.

Changes to the Cu oxidation state were observed using hard x-ray nanoprobe fluorescence microscopy and were correlated with the room temperature charge transport behavior. Our study could provide insights for device applications because multi-order of magnitude resistance switching, in which regions of oxide are fully reduced to metal, can involve mechanical damage to the top electrode and high local temperatures that cause unwanted thermal diffusion.[12,13]

The samples analyzed in these experiments consisted of SiN/Ti/Pt/40 nm CuO_x/Pt. Reactive RF magnetron sputtering was used to deposit the oxide layer from a Cu target, resulting in oxygen-deficient CuO that we will refer to as CuO_x. The top Pt electrodes were 2 μm in diameter and we refer to the region of the sample under the top electrode as the 'pad'. The x-ray nanoprobe fluorescence microscopy and spectro-microscopy experiments were performed at the Advanced Photon Source Sector 26-ID in the Center for Nanoscale Materials, Argonne National Laboratory. A Fresnel zone plate was used to achieve a spatial resolution of 80 nm. Beam energies in a range from 8969 eV to 8999 eV were used to measure the fluorescence intensity of the Cu K-alpha peak at each scan point. Conducting-atomic force microscopy (C-AFM) was used for electrical probing in order to prevent damage to the thin SiN membranes. The SET operation, performed at negative bias, switches a pad from the high resistance state (HRS) to the low resistance state (LRS). The RESET operation, performed at positive bias, switches a pad from the LRS back to the HRS (See the supplementary information[14] for more experiment details).

FIG. 1 shows bipolar current-voltage curves for two SiN/Ti/Pt/CuO_x/Pt heterostructures: (a) Pad 1 and (b) Pad 2. In both cases the curves show a repeatable bipolar resistance switching process with clear hysteresis. Despite the difference in compliance current (600 µA for Pad 1 and 900 µA for Pad 2) the shapes of the I-V curves are very similar, with an asymmetry between the positive voltage (RESET) curve and the negative voltage (SET) curve. The resistance ratio (R_{HRS}/R_{LRS}) was calculated at a voltage of 0.5 V for each heterostructure, giving values of 2.8 for Pad 1 and 4.8 for Pad 2.

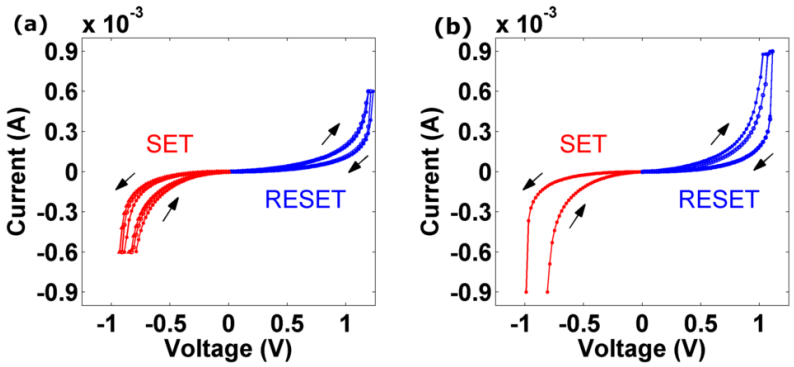

FIG. 1. *I-V curves for (a) Pad 1 (b) Pad 2. After gradual electroforming, both pads repeatedly switch between high and low resistance states.*

In order to explore possible changes to the Cu oxidation state between the LRS and HRS, single energy x-ray fluorescence maps were collected on three different SiN/Ti/Pt/CuO_x/Pt heterostructures as shown in Figure 2(a–c). Pad 0 was scanned in its as-prepared state. Transport measurements made on other heterostructures shows that the as-prepared pads are in the HRS. After several resistance switching cycles, Pad 1 was scanned in the LRS and Pad 2 was scanned in the HRS. The fluorescence maps were normalized so that the scan points in the off-pad region for each map have the same average intensity. The active heterostructure region can be observed

from the reduction in intensity of the Cu K-alpha signal, which results from the presence of the top Pt electrode. The exact position of the top electrode edge was determined from the Pt fluorescence map and is indicated on each map by the dotted outline. We are confining our analysis to a sub-region modified by the applied electric field, indicated on each map with a solid outline. We excluded the regions near the pad edges to exclude variations that can result from edge roughness or changes in thickness.

We can assume that the variation in Cu K-alpha intensity across the pad region (area under the top electrode) shows a normal distribution if the composition of the CuO_x layer and the thickness of the Pt top electrode are relatively homogeneous. In order to look for regions that show statistically distinct Cu fluorescence intensity, the distribution of Cu fluorescence intensity was plotted for each of the three pads using a normal probability plot as shown in Fig. 2(d–f). For Pad 0 (as-prepared, HRS) and Pad 2 (HRS after RESET), 99.8% of the points follow a linear trend line in the probability plot, which indicates that the Cu fluorescence data are well described by a normal distribution. For Pad 1, which is in the LRS, 98% of the points in the probability plot follow a linear trend, but there are 2% of points at the extremes of the distribution with fluorescence intensity that is noticeably higher than would be expected for a normal distribution.

The magnitude of the residual between the measured intensity and the statistically-modeled intensity (straight line shown on each normal probability plot) can thus be used to identify the location of scan points at which the Cu K-alpha fluorescence intensity is statistically greater than the expected distribution, as shown in Fig. 2(g–i). Pad 1 (LRS), shows several clusters of scan points with high Cu intensity and with a cluster size from 150 to 200 nm. However, Pads 0 and 2 (HRS), show relatively few scan points with high Cu intensity. Thus,

there is a clear correlation between local regions with high Cu intensity and a low resistance state for the Pt/CuO_x/Pt heterostructure.

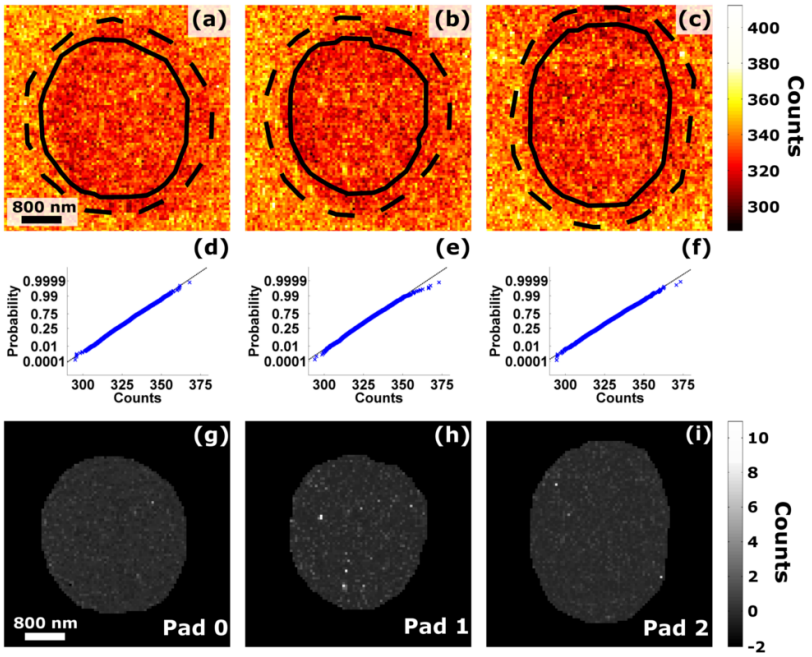

FIG. 2. (a, b, c) Cu K-alpha fluorescence maps, (d, e, f) normal probability plots of Cu K-alpha fluorescence counts, and (g, h, i) maps of difference between measured Cu fluorescence counts at each point and the counts modeled by a normal distribution for (a, d, g) HRS as-prepared, (b, e, h) LRS after SET, (c, f, g) HRS after RESET (a, b, c).

In order to explore in more detail the possible variations in stoichiometry of the CuO_x for the higher fluorescence intensity regions in the LRS, we performed x-ray fluorescence spectro-microscopy on the lower left corner of Pad 1. The resulting set of Cu K-alpha fluorescence maps obtained at a series of incident energies can also be thought of as a 2D map of Cu K-alpha fluorescence spectra. FIG. **3**(a) shows an example of a Cu K-alpha fluorescence spectrum from a single scan point, together with the pad-averaged spectrum and vertical lines indicating the ±3σ distribution width at each energy. Each value in the pad-averaged spectrum was obtained by

averaging over all scan points within the selected region under the top Pt electrode at a particular incident energy.

An average percent difference map, as shown in Fig. 3(b), was created to identify locations across the pad at which the Cu K-alpha peak has higher intensity than the pad-averaged peak. The values in Fig. 3(b) were computed according to Eq. (1):

$$D^{avg}(\mathrm{x},\mathrm{y}) = \frac{1}{n}\sum_{E=8969}^{8999}\frac{I_E(x,y) - I_E^{pad}}{I_E^{Pad}} \times 100 \qquad (1)$$

where I_E is the fluorescence intensity at photon energy E and position (x,y) and I_E^{pad} is the fluorescence intensity at photon energy E averaged over the region shown in Fig 3(b) that is under the Pt electrode. The sum is over the incident photon energy values used (n=21, in steps of 1.5 eV). The red/orange regions shown in Fig. 3(b) indicate scan points at which the local Cu K-alpha fluorescence peak has higher intensity than the pad-averaged peak. As can be seen, a single 160 nm size region, indicated by the arrow, is observed at which the intensity is > 4.4% higher than the pad average.

The x-ray spectro-microscopy results confirm that regions of higher Cu K-alpha fluorescence intensity in the single energy maps shown in Fig. 2 also show higher Cu K-alpha across the entire peak edge. Several x-ray absorption studies in the literature have shown that x-ray absorption across the Cu K-edge increases as CuO is reduced to Cu_2O and to Cu.[15–17] Although the detailed shape of our Cu K-alpha fluorescence edge is not identical to those seen using x-ray absorption, we assume that this trend applies qualitatively within this range of incident photon energy.[18] As a result, we can conclude that within the spots of higher Cu K-alpha fluorescence intensity, the CuO_x has been partially reduced to CuO_y where 1>x>y.

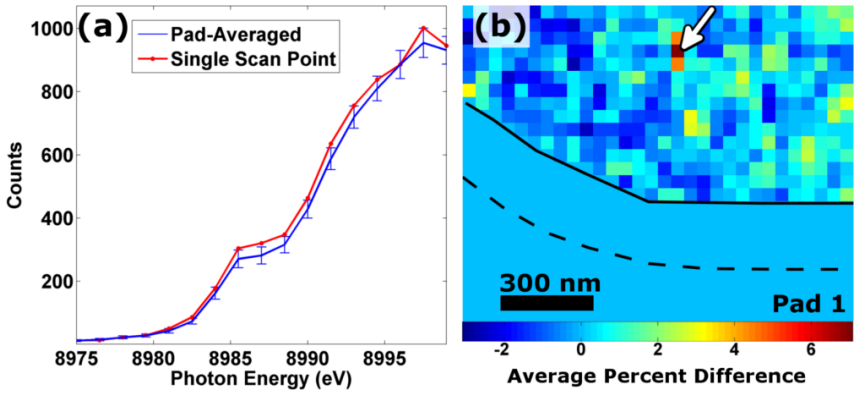

FIG. 3. *X-ray Nanoprobe Spectro-Microscopy: (a) a Cu K-alpha fluorescence spectra and (b) map of the average percent differences of Cu K-alpha fluorescence intensity as defined above. These data were collected from the bottom left corner of Pad 1.*

In order to better explain the correlation between electrical resistance state and the presence of reduced CuO_x, we first assume that the LRS consists of a CuO_x matrix and CuO_y conductive bridges ($1 > x > y$). The total resistance R_{tot} is modeled in Eq. (2) in terms of a bridge resistance R_b and a matrix resistance R_m connected in parallel. In the HRS, R_{tot} equals R_m, whereas in the LRS, R_{tot} is $< R_m$ by a factor *f,* which is defined as the total resistance ratio (R_{HRS}/R_{LRS}).

$$R_{tot} = \frac{R_b R_m}{R_b + R_m} = \left(\frac{1}{f}\right) R_m \qquad (2)$$

We assume that current flows homogeneously through the bridge and matrix of thickness t and area A_b and A_m respectively. The areas were measured from the x-ray microscopy data and the thickness from a cross-section transmission electron microscopy image shown in Fig. S2.

Thus R_b and R_m in Eq. (2) can be substituted by ρ_b and ρ_m and the appropriate values of t, A_b, and A_m. The oxide resistivity ratio (matrix/bridge, ρ_m/ρ_b) can now be found by solving Eq.(2) with these substitutions:

$$\frac{\rho_m}{\rho_b} = (f-1)\frac{A_m}{A_b} \qquad (3)$$

We can use Eq. (3) to estimate the oxide resistivity ratio and infer the extent of the CuO_x reduction in the LRS bridges. Assuming that conductive bridges occupy only 2% of the pad area ($A_b / A_m = 0.02$), the observed factor of four decrease in the pad resistance can be accounted for if the conductive bridges oxide, CuO_y has a resistivity that is a factor of 150 less than that of the matrix. According to the literature, the resistivity of Cu_2O and CuO can each vary over three orders of magnitude. Cu_2O has the highest maximum resistivity, followed by CuO and then Cu metal.[19] However, it was also shown that the resistivity of oxygen-depleted CuO is an order of magnitude higher than that of oxygen-rich Cu_2O.[19,20] These results agree with our oxide resistivity ratio estimate, suggesting that we have indeed stayed within a regime where we are changing the oxidation state of the Cu oxide without reducing it to Cu metal.

Although a local reduction of CuO_x creates regions (bridges) of lower resistivity, our I-V curves show that the LRS is not metallic. In order to determine the conduction mechanism for both states, the current-voltage data were plotted in a way that displays a linear trend line if the governing equation for a particular conduction mechanism is obeyed. The conduction mechanisms tested were Schottky, Frenkel-Poole emission, space-charge limited current, and Fowler-Nordheim tunneling. The best agreement with the data was for Schottky emission, whose governing equation is the modified Richardson equation given by[21]:

$$J = A_G T^2 e^{\frac{-\left(\Delta E - \sqrt{\frac{e^3 F}{4\pi\varepsilon}}\right)}{kT}} \quad (4)$$

Here J is the current density, T is the absolute temperature, ΔE is effective Schottky barrier height, F is the electric field, and ε is the dielectric constant.

Fig. 4 shows plots of ln (J) vs. √(|F|) calculated from the I-V data for Pad 1 (a) and Pad 2 (b). Note that plots for negative bias show the same result. The high voltage and very low voltage regimes of the current-voltage curves were not fitted. In all cases, there is a strong agreement with the linear fit lines, which supports Schottky emission as the conduction mechanism. The y-intercepts of the linear fit lines can be used to estimate the effective Schottky barrier height of the Pt/CuO_x/Pt heterostructures for each resistance state and these data are shown within Fig. 4. The change in Schottky barrier height between the HRS and LRS is about 0.04 eV. Assuming that the linear fit residuals are normally distributed, the barrier heights have a 95% confidence interval of ± 0.001 eV.

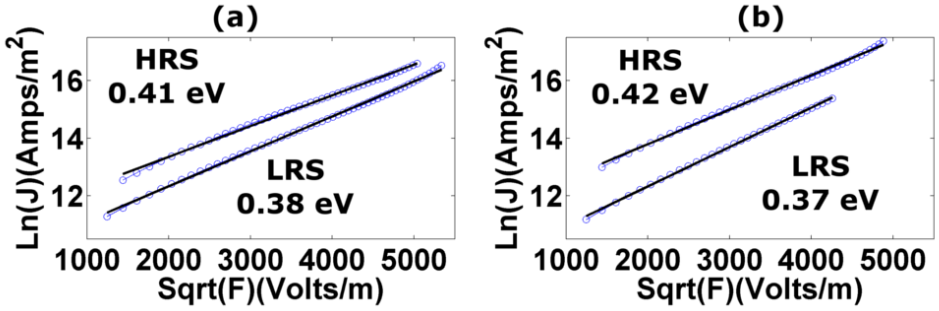

FIG. 4. Plots of ln (J) vs √(F): (a) Pad 1, positive bias, and (b) Pad 2, positive bias.

The Schottky barrier height for Pt/CuO_x will depend on the difference in work functions and majority carrier type. The work function of Pt ranges from 5.6 to 6.1 eV.[22] The work function of CuO ranges from 4.5 to 6.1 eV depending on the deposition conditions.

Stoichiometric CuO is known to be a p-type semiconductor but n-type CuO has also been observed, depending on the preparation method.[11,23] As a result of these processing dependent variations, the presence of a Schottky barrier at the Pt/CuO_x interfaces could be due to either p-type CuO with higher work function than Pt or n-type CuO with lower work function than Pt.

Our hypothesis is that the CuO_x in this experiment is p-type and has a work function higher than that of Pt (see Fig. S1 for the proposed energy level schematic).[10] This hypothesis is consistent with the result from Greiner *et al.* that the work function of CuO_x decreases with decreasing oxidation state.[24] For p-type CuO_x with a higher work function than Pt, the partial reduction to CuO_y will decrease the work function and lower the Schottky barrier height, as shown in Fig. 4. However, if the CuO_x was n-type with a lower work function than Pt, the partial reduction to CuO_y would further decrease the work function and increase the Schottky barrier height, which is not observed.

We therefore propose the following model to explain the correlated resistance and oxidation state changes observed in Pt/CuO_x/Pt heterostructures in the absence of a metallic conducting path. In the as-prepared state, the CuO_x is oxygen deficient with many oxygen vacancies and a Schottky barrier at the top and bottom Pt/CuO_x interfaces. During mild electroforming at negative voltage, oxygen anions migrate into the bottom Pt electrode. Regions in which oxygen migration has occurred become partially reduced and this lowers the CuO_x work function.[24] As a result, the Schottky barrier height becomes lower and the LRS is achieved. Under positive voltage, the oxygen anions migrate from the bottom electrode back into the CuO_y and the HRS is achieved once the original Schottky barrier height is restored.

We believe that this mechanism of resistance switching in Pt/CuO_x/Pt heterostructures is an early stage of the redox-based resistance switching previously reported, in which a metallic

conduction path is formed.[10] Our study demonstrates the role of the Schottky barrier at the Pt/CuO_x interfaces on the resistance switching process in the absence of a metallic conduction path, and we propose that performing resistance switching in this regime could lead to more reliable switching behavior for resistance-change based memory devices or bio-inspired artificial neuron devices.

In conclusion, we showed that there is a partial reduction of the as-prepared CuO_x when changing from HRS to LRS. Our results show that the dominant conduction mechanism is Schottky emission and that the effective barrier height scales with the resistance state of the heterostructure. Our model for resistance switching in Pt/CuO_x/Pt heterostructures in the absence of a metallic conducting path is based on the electric field driven migration of oxygen anions that electrochemically reduce/oxidize the CuO_x. This leads to modulation of both the local CuO_x resistivity and the effective Schottky barrier height.

The work was supported by the U.S. Department of Energy, Office of Science, Materials Sciences and Engineering Division. We acknowledge use of the Center for Nanoscale Materials, a U.S. Department of Energy, Office of Science, Office of Basic Energy Sciences User Facility under Contract No. DE-AC02-06CH11357.

References

[1] S. Seo, M.J. Lee, D.H. Seo, E.J. Jeoung, D.-S. Suh, Y.S. Joung, I.K. Yoo, I.R. Hwang, S.H. Kim, I.S. Byun, J.-S. Kim, J.S. Choi, and B.H. Park, Appl. Phys. Lett. **85**, 5655 (2004).

[2] D.-H. Kwon, K.M. Kim, J.H. Jang, J.M. Jeon, M.H. Lee, G.H. Kim, X.-S. Li, G.-S. Park, B. Lee, S. Han, M. Kim, and C.S. Hwang, Nat. Nanotechnol. **5**, 148 (2010).

[3] O. Heinonen, M. Siegert, A. Roelofs, A. K. Petford-Long, M. Holt, K. d'Aquila, and W. Li, Appl. Phys. Lett. **96**, 103103 (2010).

[4] S.H. Chang, J. Kim, C. Phatak, K. D'Aquila, S.K. Kim, J. Kim, S.J. Song, C.S. Hwang, J.A. Eastman, J.W. Freeland, and S. Hong, ACS Nano **8**, 1584 (2014).

[5] S.H. Jo, T. Chang, I. Ebong, B.B. Bhadviya, P. Mazumder, and W. Lu, Nano Lett. **10**, 1297 (2010).

[6] R. Waser and M. Aono, Nat. Mater. **6**, 833 (2007).

[7] J.J. Yang, D.B. Strukov, and D.R. Stewart, Nat. Nanotechnol. **8**, 13 (2013).

[8] P. Zhou, H.B. Lv, M. Yin, L. Tang, Y.L. Song, T. a. Tang, Y.Y. Lin, A. Bao, A. Wu, S. Cai, H. Wu, C. Liang, and M.H. Chi, J. Vac. Sci. Technol. B Microelectron. Nanom. Struct. **26**, 1030 (2008).

[9] R. Dong, D.S. Lee, W.F. Xiang, S.J. Oh, D.J. Seong, S.H. Heo, H.J. Choi, M.J. Kwon, S.N. Seo, M.B. Pyun, M. Hasan, and H. Hwang, Appl. Phys. Lett. **90**, 042107 (2007).

[10] R. Yasuhara, K. Fujiwara, K. Horiba, H. Kumigashira, M. Kotsugi, M. Oshima, and H. Takagi, Appl. Phys. Lett. **95**, 012110 (2009).

[11] S.-J. Choi, G.-S. Park, K.-H. Kim, W.-Y. Yang, H.-J. Bae, K.-J. Lee, H. Lee, S.Y. Park, S. Heo, H.-J. Shin, S. Lee, and S. Cho, J. Appl. Phys. **110**, 056106 (2011).

[12] J.P. Strachan, D.B. Strukov, J. Borghetti, J.J. Yang, G. Medeiros-Ribeiro, and R.S. Williams, Nanotechnology **22**, 254015 (2011).

[13] J. Joshua Yang, F. Miao, M.D. Pickett, D. a a Ohlberg, D.R. Stewart, C.N. Lau, and R.S. Williams, Nanotechnology **20**, 215201 (2009).

[14] See supplementary material for details on the experimental procedures, (n.d.).

[15] X. Wang, J.C. Hanson, A.I. Frenkel, J.-Y. Kim, and J. a. Rodriguez, J. Phys. Chem. B **108**, 13667 (2004).

[16] J.Y. Kim, J. a Rodriguez, J.C. Hanson, A.I. Frenkel, and P.L. Lee, J. Am. Chem. Soc. **125**, 10684 (2003).

[17] a Gaur, B.D. Shrivastava, and S.K. Joshi, J. Phys. Conf. Ser. **190**, 012084 (2009).

[18] R. Kurian, K. Kunnus, P. Wernet, S.M. Butorin, P. Glatzel, and F.M.F. de Groot, J. Phys. Condens. Matter **24**, 452201 (2012).

[19] V.F. Drobny and L. Pulfrey, Thin Solid Films **61**, 89 (1979).

[20] L. De Los Santos Valladares, D.H. Salinas, a. B. Dominguez, D.A. Najarro, S.I. Khondaker, T. Mitrelias, C.H.W. Barnes, J.A. Aguiar, and Y. Majima, Thin Solid Films **520**, 6368 (2012).

[21] M.E. Kiziroglou, X. Li, a. a. Zhukov, P. a. J. de Groot, and C.H. de Groot, Solid. State. Electron. **52**, 1032 (2008).

[22] F. Gossenberger, T. Roman, K. Forster-Tonigold, and A. Groß, Beilstein J. Nanotechnol. **5**, 152 (2014).

[23] W. Siripala and J. Jayakody, Sol. Energy Mater. **14**, 23 (1986).

[24] M.T. Greiner, L. Chai, M.G. Helander, W.-M. Tang, and Z.-H. Lu, Adv. Funct. Mater. **22**, 4557 (2012).